ACS Catalysis

Research Article

Cite This: ACS Catal. 2019, 9, 2091−2100

pubs.acs.org/acscatalysis

Selective Earth-Abundant System for CO_2 Reduction: Comparing Photo- and Electrocatalytic Processes

Christoph Steinlechner,[†] Arend F. Roesel,[‡,∇] Elisabeth Oberem,[†,‡,∇] Ayla Päpcke,[§,∇] Nils Rockstroh,[†] Frédéric Gloaguen,[∥] Stefan Lochbrunner,[§,∇] Ralf Ludwig,[†,‡,∇] Anke Spannenberg,[†] Henrik Junge,[†] Robert Francke,*[,‡,∇] and Matthias Beller*[,†]

[†]Leibniz Institute for Catalysis at the University of Rostock, Albert-Einstein-Straße 29a, 18059 Rostock, Germany

[‡]Institute of Chemistry, Rostock University, Albert-Einstein-Staße 3a, 18059 Rostock, Germany

[§]Institute of Physics, Rostock University, Albert-Einstein-Staße 23-24, 18059 Rostock, Germany

[∇]Department Life, Light & Matter, Rostock University, Albert-Einstein-Straße 25, 18051 Rostock, Germany

[∥]UMR 6521, CNRS, Université de Bretagne Occidentale, CS 93837, 29238 Brest, France,

Supporting Information

ABSTRACT: The valorization of CO_2 via photo- or electrocatalytic reduction constitutes a promising approach toward the sustainable production of fuels or value-added chemicals using intermittent renewable energy sources. For this purpose, molecular catalysts are generally studied independently with respect to the photo- or the electrochemical application, although a unifying approach would be much more effective with respect to the mechanistic understanding and the catalyst optimization. In this context, we present a combined photo- and electrocatalytic study of three Mn diimine catalysts, which demonstrates the synergistic interplay between the two methods. The photochemical part of our study involves the development of a catalytic system containing a heteroleptic Cu photosensitizer and the sacrificial BIH reagent. The system shows exclusive selectivity for CO generation and renders turnover numbers which are among the highest reported thus far within the group of fully earth-abundant photocatalytic systems. The electrochemical part of our investigations complements the mechanistic understanding of the photochemical process and demonstrates that in the present case the sacrificial reagent, the photosensitizer, and the irradiation source can be replaced by the electrode and a weak Brønsted acid.

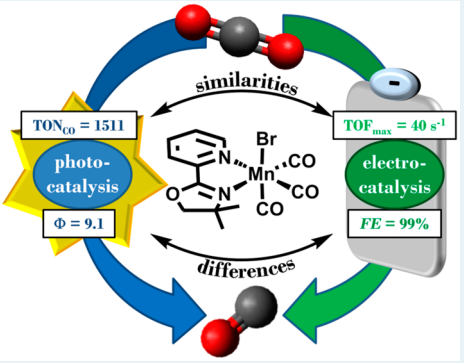

KEYWORDS: *carbon dioxide utilization, photocatalysis, electrocatalysis, manganese, copper*

1. INTRODUCTION

Inspired by natural photosynthesis, the direct utilization of sunlight for conversion of CO_2 into solar fuels and/or chemicals represents an attractive opportunity to substitute fossil fuels.[1] In this context, interesting options are photo-[2] and electrocatalytic[3] conversions of CO_2 into C_1 intermediates such as formic acid or carbon monoxide, which can be further processed to fuels or value-added products.

Initiated by the seminal work of Lehn and co-workers, a plethora of photo- and electrocatalytic systems for CO_2 reduction based on transition metal complexes have been established.[3,4] In general, a catalyst (Cat) for CO_2 ligation and its subsequent reduction, a sacrificial donor (SD) which provides both electrons and protons for the reduction, and a photosensitizer (PS) as light-harvesting unit are employed in photocatalytic systems. Due to their strong spin−orbit-coupling (SOC, correlates with the atomic number, SOC ∼ Z^4) and the resulting excited long-living triplet states (^{3}MLCT) together with their strong reduction power, noble metals such as Ru and Ir, usually as polypyridyl and cyclometalated complexes, are commonly applied as PS.[5] Furthermore, Ru, Ir, and Re have been employed as metal centers for CO_2 reduction catalysts. However, due to the high cost and low abundancy, there is an increasing interest in substituting such precious metals by non-noble metals for both Cat and PS.[4] Similar trends have also been followed in the field of electrocatalytic CO_2 reduction, where Re,[6] Ru,[7] and Pd[8] catalysts have been replaced by more abundant metals such as Fe,[9] Ni,[10] Co,[11] and Mn.[12] The first light-driven reduction of CO_2 using a molecularly defined Mn catalyst was reported by Ishitani and co-workers in 2014. Using *fac*-Mn(bpy)(CO)$_3$Br (bpy = 2,2′-bipyridine) as Cat, Ru(bpy)$_3$ as PS and 1,3-dimethyl-2-phenyl-2,3-dihydro-1*H*-benzo[d]imidazole (BIH) as SD in DMF (dimethylformamide)/TEOA (triethanolamine) (25% vol. TEOA), formate was obtained as the main product (TON_{HCOOH} = 157) along with carbon monoxide

Received: September 13, 2018
Revised: December 10, 2018
Published: January 11, 2019

(TON_{CO} = 12) and hydrogen (TON_{H2} = 8) as side products. By substitution of DMF with CH_3CN, the formation of formate was drastically reduced (TON_{HCOOH} = 78), whereby the formation of carbon monoxide and hydrogen (TON_{CO} = 40; TON_{H2} = 17) was promoted.[13] Later on, Bian et al. developed a system exclusively based on non-noble metals where Zn^{II}-TPP (TPP = tetraphenylporphyrin) was applied as PS and Mn(phen)$(CO)_3$Br (phen = phenanthroline) as Cat (see Chart 1).[14] Following this work, the group of Ishitani

Chart 1. Earth Abundant Photocatalytic Systems for CO_2-to-CO Conversion

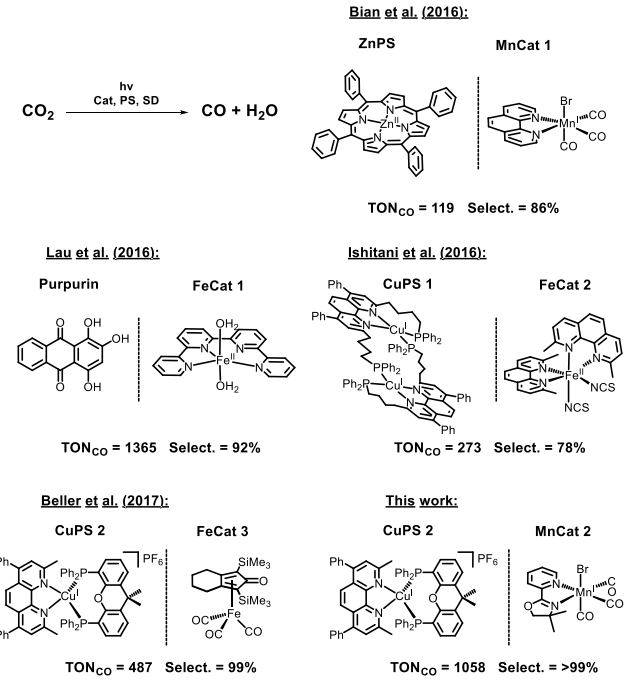

reported the combination of $Fe^{II}(dmp)_2(SCN)_2$ (dmp = 2,2′-dimethylphenanthroline) with a dimeric CuPS.[15] While all these systems also generate hydrogen by proton reduction as a competing process, some of us reported a more chemoselective CO generation using a combination of iron-cyclopentadienone and *in situ*-generated heteroleptic Cu complexes (see Chart 1).[16] As an alternative to non-noble metal based photosensitizers, the use of organic dyes as light harvesting units was also reported.[17] As an example Guo et al. published a combination of a purpurin PS, BIH as SD, and Fe(qpy)$(H_2O)_2$ as well as Co(qpy)$(H_2O)_2$ (qpy = quaterpyridine) as Cat. The CO_2 reduction was carried out in DMF and led to CO formation in 92% selectivity (TON_{CO} = 1365).[18]

Herein we report a new fully earth-abundant photocatalytic system for the conversion of CO_2 to CO. It is based on novel manganese diimine complexes **1**−**3** (see Chart 2) in conjunction with a heteroleptic CuPS. We complement these results with an electrochemical study of **1**−**3** in order to probe the transferability of the photo- to the electrocatalytic process and to highlight differences and similarities. In addition, spectroscopic and mechanistic experiments are performed to gain insight into the reaction path.

2. RESULTS AND DISCUSSION

2.1. Development of the Photocatalytic Procedure. Following previous studies using a copper−iron-system (1.0

Chart 2. Top: Novel Manganese(I) Diimine Complexes 1 [Mn(pyrox)$(CO)_3$Br], 2 [Mn(benzox)$(CO)_3$Br], and 3 [Mn(qinox)$(CO)_3$Br] for CO_2 Reduction. Bottom: Molecular Structures of 1 and 3 Obtained via Single Crystal X-ray Diffraction (Displacement ellipsoids correspond to 30% probability. Hydrogen atoms are omitted for clarity; for more details see SI)

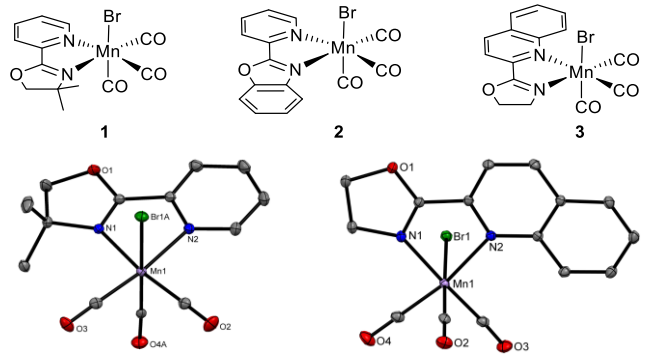

μmol Cat, 5.0 μmol $[Cu(CH_3CN)_4]PF_6$, 5.0 μmol bathocuproine, and 15.0 μmol xantphos),[16] we started our investigations with a careful optimization of the reaction conditions, whereby the influences of the catalyst loading, the solvent, and the ratio between Cat and PS were varied. The reactions were carried out in CH_3CN in the presence of BIH and TEOA, with the latter ones acting as sacrificial electron and proton donors, respectively.[19] Important key experiments are summarized in Table 1.

Table 1. Photocatalytic Optimization and Catalyst Screening[a]

Entry	Cat	Mn μmol	Cu μmol	Mn/Cu Ratio	Cu/NN/PP Ratio	TON_{CO}[b]
1	**1**	0.1	0.2	1/2	1/1/3	27
2	**1**	0.1	0.5	1/5	1/1/3	90
3	**1**	0.1	1.0	1/10	1/1/3	460
4	1	0.2	1.0	1/5	1/1/3	461
5	**1**	0.01	1.0	1/100	1/1/3	659
6[c]	**1**	0.01	1.0	1/100	1/1/3	1058
7[d]	**1**	0.01	1.0	1/100	1/1/3	1511
8	**2**	0.01	1.0	1/100	1/1/3	113
9	**3**	0.01	1.0	1/100	1/1/3	0

[a]Reaction conditions: PP = xantphos; NN = bathocuproine; Cu = $[Cu(CH_3CN)_4]PF_6$, 0.1 M BIH in 10 mL CO_2 saturated CH_3CN/TEOA (5:1, v/v); Hg-lamp (light output 70 mW) equipped with a 415 nm band-pass filter; time of irradiation = 3 h. [b]All TONs are calculated based on [Mn]. [c]Time of irradiation = 5 h. [d]Addition of 1.0 μmol of $[Cu(CH_3CN)_4]PF_6$ after 5 h; time of irradiation = 10 h.

The best results (TON_{CO} = 1058 with a selectivity of >99% and a quantum yield (Φ) of 0.47%; the use of a higher catalyst loading results in Φ = 9.1%; for details see Supporting Information) were obtained using catalyst **1** with a loading of 0.01 μmol in 10 mL of CH_3CN/TEOA (5:1, v/v), a Cat/CuPS ratio of 1/100, and 5 h of irradiation with monochromatic light at λ = 415 nm and a power output of 70 mW (Table 1, entry 6). Applying the same conditions, the activity of catalyst **2** was drastically reduced (TON_{CO} = 113), whereby the selectivity remained high (>99%). In contrast, no CO formation was observed employing catalyst **3** (Table 1, entry 8−9). For the *in situ*-generation of the CuPS 1.0 μmol

DOI: 10.1021/acscatal.8b03548
ACS Catal. 2019, 9, 2091−2100

$[Cu(CH_3CN)_4]PF_6$, an equimolar amount of bathocuproine and a 3-fold excess of xantphos were used in order to avoid the formation of the less active homoleptic $Cu(NN)_2$ complex.[16,20] Under these conditions, the H_2 formation was below the quantification limit (TON_{H2} < 1) and formate was not detected. Upon substitution of the *in situ* formed CuPS by the molecularly defined $[Cu(xantphos)(bathocuproine)]PF_6$, the Mn catalyst turnover numbers were diminished by approximately 100 resulting in a TON_{CO} of 551, while the selectivity of >99% still remained high (Table 2, entry 1). By performing

Table 2. Control Experiments for the Photocatalytic CO_2 Reduction Catalyzed by 1

Entry	1 μmol	CuPS μmol	SD	TON_{CO}[b]
1[c]	0.01	mol. def. 1.0	BIH + TEOA	551
2[d]	0.01	1.0	BIH + TEOA	2
3	-	1.0	BIH + TEOA	0
4	0.01	-	BIH + TEOA	5
5[e]	0.1	1.0	BIH + TEOA	0
6[f]	0.01	1.0	BIH + TEOA	0
7	0.01	1.0	TEOA	0
8	0.01	1.0	BIH	31
9[g]	0.01	1.0	BIH + TEOA	700

[a]Reaction conditions: 3 μmol xantphos; 1 μmol of bathocuproine; 0.1 M BIH, and 1.0 μmol of $[Cu(CH_3CN)_4]PF_6$ in 10 mL of CO_2 saturated CH_3CN/TEOA (5:1, v/v); Hg-lamp (light output 70 mW) equipped with a 415 nm band-pass filter; time of irradiation = 3 h. [b]All TON are calculated based on [Mn]. [c]The molecularly defined CuPS ($[Cu(xantphos)(bathocuproine)]PF_6$) was used. [d]Ar atmosphere. [e]NMP/TEOA (5:1, v/v). [f]Dark reaction. [g]Hg poisoning.

a control experiment under Ar atmosphere, it was confirmed that neither formate, H_2, nor CO are formed in the absence of CO_2 (Table 2, entry 2). Correspondingly, no reaction was observed when either the catalyst or the CuPS were omitted, when acetonitrile (CH_3CN) was replaced by *N*-methyl-2-pyrrolidone (NMP), or the reaction was performed in the dark (Table 2, entries 3−6). The TON was drastically decreased using only TEOA or BIH as SD (Table 2, entries 7−8). Therefore, we conclude that every component is vital for this light-driven, proton-coupled CO_2 reduction. Carbon isotope labeling experiments using $^{13}CO_2$ were performed to ensure that the evolved CO originates from CO_2 (confirmed by GC-MS analysis).

The progression of the TON_{CO} over time showed a deactivation of the catalytic system after 5 h of irradiation (Figure 1, black dots). However, the addition of 1.0 μmol Cu precursor after 5 h induced a reactivation of the process for a further 5 h (Table 1, entry 7 and Figure 1, red circles). The restart of the process adding only the Cu precursor strongly indicates a transformation of the active Cu(I) PS into a flattened Cu(II) complex and subsequent exciplex quenching upon light irradiation, which is inactive for the light driven electron transfer.[21b] Additionally, disintegration of the catalyst losing CO ligands by light induced Mn-CO bond cleavage was observed by IR measurements before and after irradiation of an acetonitrile solution containing **1**, **2**, or **3** with 415 nm for 10 min (see Figure S2).

Notably, in the course of every reaction performed in CH_3CN/TEOA (5:1, v/v), we observed the formation of black particles, which then were dissolved in the reaction mixture within a few hours after irradiation. Some of the particles

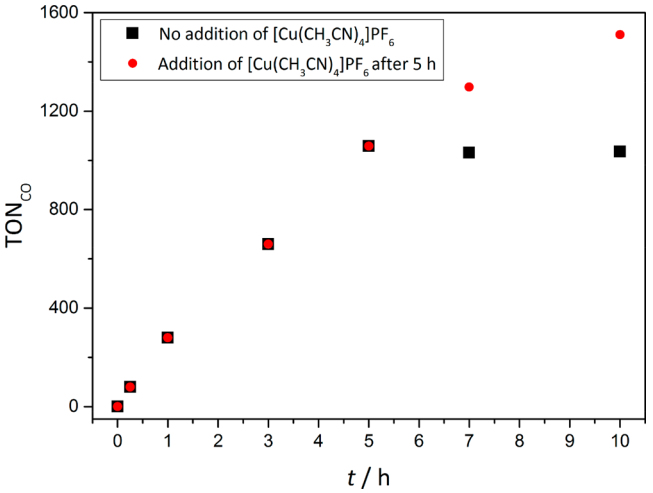

Figure 1. Progress of photocatalytic CO generation over time. Reaction conditions: 0.01 μmol of **1**; 3 μmol of xantphos; 1 μmol of bathocuproine; 0.1 M BIH and 1.0 μmol of $[Cu(CH_3CN)_4]PF_6$ in 10 mL of CO_2 saturated CH_3CN/TEOA (5:1, v/v); Hg-lamp (light output 70 mW) equipped with a 415 nm band-pass filter. After 5 h 1.0 μmol of $[Cu(CH_3CN)_4]PF_6$ was added (red circles).

precipitated on a stirring bar possessing a roughened surface (Figure S8) and thus allowed for the analysis with Raman spectroscopy. The measured Raman bands match with the reference data for copper(I)oxide (Cu_2O, see Figure S9).[21] To investigate whether the photocatalytic process is a homogeneous or a Cu_2O-catalyzed heterogeneous one, mercury poisoning experiments were carried out, in which no influence on the catalytic activity was observed (Table 2, entry 9). Complementarily, we performed catalyst poisoning experiments by addition of various equivalents of trimethylphosphine (PMe_3) (0.25, 0.5, 0.75, and 1.00 equiv with respect to the catalyst). Increasing the amount of PMe_3, the carbon monoxide evolution was diminished in a linear fashion (Table S3, Figure S10). To avoid side effects of an excess of xantphos, the molecularly defined $[Cu(xantphos)(bathocuproine)]PF_6$ PS was used for PMe_3 poisoning. Interestingly, stirring a mixture of commercially available Cu_2O powder, bathocuproine, and xantphos in dry CH_3CN overnight led to the formation of the heteroleptic $[Cu(NN)(PP)]^+$ complex demonstrated by its characteristic ^{31}P NMR signal at δ = 26.1 ppm (Figure S12) and by high resolution ESI-MS (Figure S13). In photocatalytic experiments using **1** and Cu_2O as PS precursor instead of $[Cu(CH_3CN)_4]PF_6$, carbon monoxide was selectively formed with a TON_{CO} of 631 (Table S2). Notably, no CO_2 conversion was observed under the same conditions in the absence of bathocuproine and xantphos. These results demonstrate that the photocatalytic process is a homogeneous one even when starting from a heterogeneous metal precursor, although the mechanism of the intermittent Cu_2O-formation remains unclear.

2.2. Luminescence Quenching Experiments. For elucidation of the mechanism of the photoinduced electron transfer, we carried out quenching experiments of the excited state of the *in situ* generated CuPS (see Figure 2). Employing BIH, both the luminescence and the lifetime of the excited state (τ) were significantly decreased. The quenching rate k_q was determined to be 6.0×10^9 M^{-1} s^{-1} using Stern−Volmer analysis (Figure 3, for more details see Table S1). The influence of BIH on the luminescence and τ suggests a

DOI: 10.1021/acscatal.8b03548
ACS Catal. 2019, 9, 2091−2100

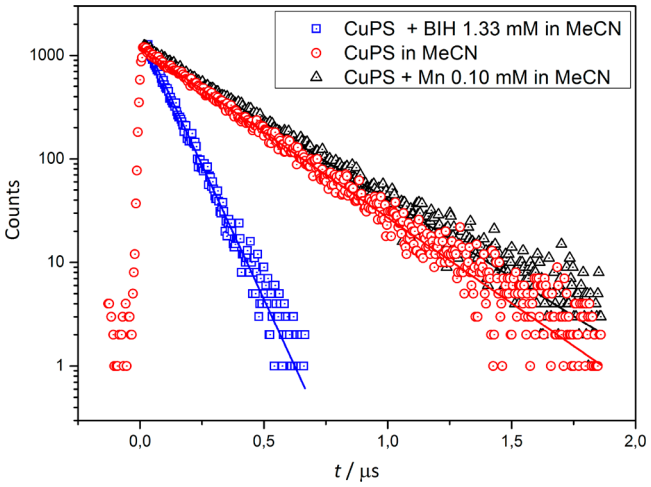

Figure 2. Luminescence decays of the CuPS in CH_3CN: CuPS in pure CH_3CN (red circles), CuPS in the presence of 0.1 mM of **1** (black triangles) and of 1.33 mM of BIH (blue squares) as quenching agent. The lines are single exponential fits revealing triplet lifetimes of 263, 290, and 84 ns for CuPS in pure CH_3CN, in the presence of **1** and of BIH, respectively.

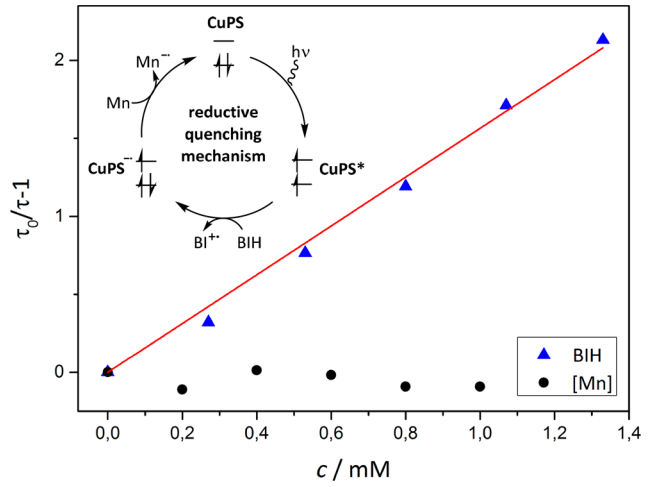

Figure 3. Stern–Volmer plot for quenching the excited CuPS by BIH (blue triangles) and by **1** (black dots). In the case of BIH a linear dependence with $y = 1.56x$ (red line) is observed whereas no quenching occurs adding **1** (black dots). Reductive quenching mechanism of the excited CuPS in the presence of BIH as quenching agent. Inset: schematic illustration of the reductive quenching mechanism.

dynamic quenching mode caused by a reductive process (see Figure 3). In the presence of **1** the luminescence is somewhat lowered due to the strong light absorption by the Mn catalyst (see Figure S4), whereas τ slightly increases from 263 ns in pure CH_3CN to e.g. 290 ns with 0.1 mM **1**. The same trend regarding the luminescence and τ was also observed in the presence of TEOA and absence of **1**. A possible explanation for this behavior might be that the triplet lifetime of CuPSs depends in general on the solvent.[20b]

2.3. *In Situ* IR Spectroscopic Investigation. In order to obtain information about the intermediates of the photocatalytic reduction, we carried out *in situ* IR spectroscopy under CO_2 atmosphere using a setup where the photoreactor is connected to the measurement cell within a pump cycle. The experiment was carried out with a mixture of CH_3CN/TEOA (5:1) containing 2.0 μmol of **1**, 20 μmol of $[Cu(CH_3CN)_4]$-PF_6, 20 μmol of bathocuproine, 60 μmol of xantphos, and 200 mg of BIH. The IR spectra recorded during the reaction are shown in Figure 4. Upon irradiation of the solution at λ = 415 nm, the $\tilde{\nu}_{CO}$ stretches at 2028, 1932, and 1923 cm^{-1} assigned to **1** diminish in the course of the experiment (indicated with arrows in Figure 4), while new bands at 2049, 1961, 1959, 1949, 1930, 1914, 1881, and 1857 cm^{-1} evolved. The bands at 1961, 1930, 1881, and 1857 cm^{-1} match several diimine-coordinated Mn(0) dimers reported in the literature.[22−24] Therefore, we assign these bands to Mn–Mn dimer **4** (see Table 3), which is formed after one-electron reduction of **1**.

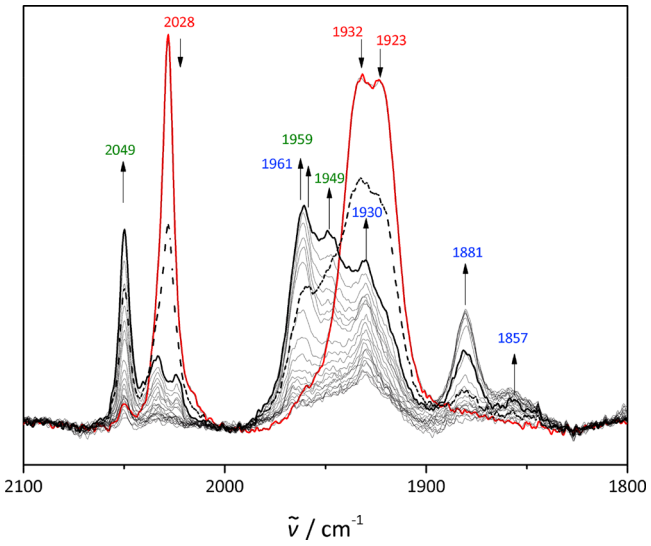

Figure 4. *In situ* IR spectroscopy of **1** in CH_3CN under CO_2, upon irradiation (415 nm, 70 mW) and in the presence of CuPS, BIH, and TEOA: Progression of the absorption spectra over time. Red line: Initial spectrum of **1**. Black line: Final spectrum after reaching a steady state. The color coding of the absorption frequencies indicates their assignment to the species shown in Table 3 (Red: species **1**, blue: species **4**, green: species **5**).

Table 3. Assignment of the IR Absorption Bands from Figure 4 to Photocatalytic Intermediates

Species	$\tilde{\nu}$/cm^{-1}			
1 $[Mn(pyrox)(CO)_3Br]$	2028	1932	1923	
4 $[Mn(pyrox)(CO)_3]_2$	1961	1930	1881	1857
$[Mn(bpy\text{-}tBu)(CO)_3]_2$[23b]	1973	1928	1878	1850
5 $[Mn(pyrox)(CO)_3S]^+$	2049	1959	1949	
S = CH_3CN	2049[a]	1958[a]	1951[a]	

[a]Solution IR spectroscopy was carried out in CH_3CN using an authentic sample of **5** (hexafluorophosphate salt).

The remaining $\tilde{\nu}_{CO}$ stretches at 2049, 1959 (overlapping with the $\tilde{\nu}_{CO}$ band 1961 cm^{-1} of **4**), and 1949 cm^{-1} can be assigned to the cationic solvent-coordinated Mn complex **5**, which was confirmed by solution IR spectroscopy of an authentic sample prepared by reaction of **1** with $AgPF_6$ (for more information see the Supporting Information). Uncoordinated CO was not

DOI: 10.1021/acscatal.8b03548
ACS Catal. 2019, 9, 2091−2100

detected in the spectra due to its poor solubility in acetonitrile, which was used as the solvent.[25]

2.4. Electrochemical Studies. One of the major challenges in homogeneous artificial photosynthesis represents the combination of CO_2 reduction and water oxidation.[25] In contrast to photocatalytic systems, which so far mostly rely on the application of SDs, electrolysis provides a straightforward alternative, since CO_2 reduction and water oxidation can be simultaneously carried out as cathodic reduction and anodic oxidation. Electrochemistry also allows for the coupling of CO_2 reduction to synthetically useful processes, e.g. the anodic synthesis of fine or bulk chemicals. This paired approach has already been successfully demonstrated employing alcohol oxidation[26] or oxidative cyclizations.[27] By definition, these paired processes can lead to Faradaic efficiencies up to 200%. Furthermore, the use of homogeneous catalysts for both processes is unproblematic when a divided cell is used.[28] In this context, exploring the electrocatalytic behavior of Mn complexes **1**−**3** toward CO_2 reduction is of particular interest. An initial screening of the catalytic activity using cyclic voltammetry (CV) showed that **1** is a very promising candidate, whereas **2** and **3** exhibit only poor activity (see Figure S24). As in the photochemical study, we have therefore focused our efforts on a thorough characterization of **1**. The electrochemical study along with a discussion of differences and similarities to the photochemical process is presented in the following.

2.5. Electrochemical Characterization of 1 under Ar. We initiated the electrochemical characterization with CV of 1 mM **1** in a 0.1 M NBu_4BF_4/CH_3CN electrolyte using a glassy carbon working electrode. The CVs recorded under Ar atmosphere at various scan rates (ν) are shown in Figure 5 (left). A quasi-reversible redox couple is centered around E = −0.94 V vs NHE with a peak-to-peak separation (ΔE_p) of 150 mV at ν = 100 mV s^{-1}. Analogously to previously reported Mn complexes with bipyridine ligands,[29] we assign the reduction signal to an ECE (electron transfer - chemical reaction - electron transfer) process. The initial single-electron reduction

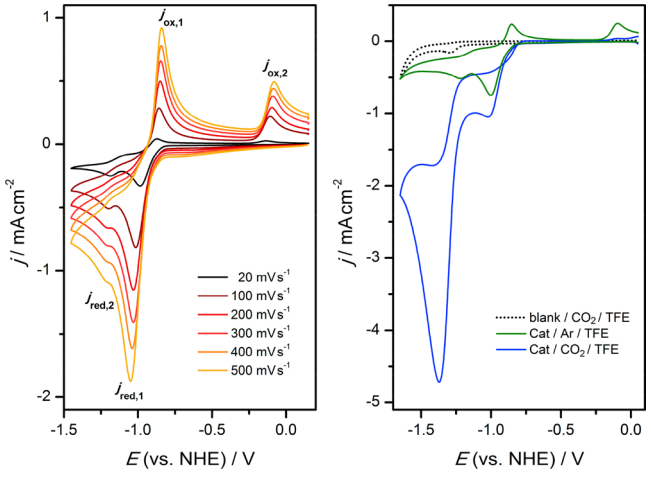

Figure 5. Cyclic voltammograms (CVs) of 1 mM **1** in 0.1 M NBu_4BF_4/CH_3CN (working electrode: glassy carbon). Left: CVs recorded at various scan rates under Ar atmosphere in the absence of a proton donor. Right: CVs recorded in the presence of 1 M 2,2,2-trifluoroethanol (TFE) at ν = 100 mV s^{-1}. Black dotted line: blank electrolyte under CO_2. Green line: 1 mM **1** under Ar, blue line: 1 mM **1** under CO_2.

is coupled to a rapid dehalogenation, which results in the formation of the radical intermediate $[Mn(pyrox)(CO)_3]^{\bullet}$. This radical is concomitantly reduced at the potential required for the reduction of **1**, leading to the formation of anionic intermediate **6**. Since the intensity $j_{ox,1}$ of the reoxidation peak is significantly diminished with respect to the reduction peak ($j_{red,1}$), it appears that a second chemical process is coupled to the initial reduction, which is relatively fast on the CV time scale. In agreement with previous reports on analogous Mn complexes,[22,23b] we assign this behavior to the dimerization of the $[Mn(pyrox)(CO)_3]^{\bullet}$ intermediate. This process also explains the appearance of a second reduction signal ($j_{red,2}$) at −1.2 V and an additional anodic peak ($j_{ox,2}$) at −0.1 V, which are characteristic for the reduction and the oxidation, respectively, of Mn−Mn dimer species.[22,23b] This interpretation is corroborated by the ν-dependency of the ratio between the peak current densities $j_{red,1}$ and $j_{red,2}$. While at small ν (long time scales), this ratio indicates that a significant fraction of radical intermediates is already dimerized upon sweeping over −1.2 V, $j_{red,2}$ diminishes relative to $j_{red,1}$ when the scan rate is increased and eventually merges into a shoulder at ν > 200 mV s^{-1}. Further evidence for the appearance of $[Mn(pyrox)(CO)_3]^{\bullet}$, **6** and Mn−Mn dimer **4** will be discussed in the context of our spectroelectrochemical investigations (*vide infra*).

2.6. Electrochemical Characterization of 1 under CO_2. We proceeded with investigating the impact of CO_2 and 2,2,2-trifluoroethanol (TFE) on the cyclic voltammetry of **1** (see Figure 5, right and Table 4). TFE was intended to play the role

Table 4. Electrocatalytic Characteristics of 1 and Reference Systems from the Literature toward CO_2 in the Presence of TFE

Catalyst	$E_{cat/2}$ [V][a]	$j_{p,cat}$ [mA cm^{-2}][a]	η_{cat} [V][b]
1	−1.29[c]	−4.7[c]	0.64
$[Mn(Mes\text{-}bpy)(CO)_3(CH_3CN)](OTf)$	−1.39[d]	−6.6[d]	0.74
$[Mn(t\text{Bu-}bpy)(CO)_3Br]$	−1.43[e]	−14.8[e]	0.78

[a]Half-wave potential vs NHE and maximum current of the catalytic wave (ν = 100 mV s^{-1}, [catalyst] = 1 mM, solvent: CH_3CN). [b]Overpotential calculated using eq 2. [c][TFE] = 1 M. [d]Extracted from Figure S14 in ref 27 ([TFE] = 1 M). [e]Extracted from Figure S4 in ref 20b ([TFE] = 0.94 M).

of the weak proton donor (in contrast to the photocatalytic experiments, where TEOA was used instead). The addition of TFE (1 M) has only a marginal influence on the voltammetric response of the Mn complex (green line in Figure 5, right), which clearly indicates that **1** is not active toward H_2 evolution under these conditions. Upon saturation of the same solution with CO_2 (blue line) the voltammetry changes significantly. While at the first reduction potential of the catalyst the cathodic peak current increases slightly, a pronounced wave with a half-wave potential $E_{cat/2}$ of −1.29 V and with a peak current density of $j_{p,\,cat}$ = −4.7 mA cm^{-2} (at ν = 100 mV s^{-1}) appears. Compared to the $[Mn(Mes\text{-}bpy)(CO)_3(CH_3CN)](OTf)$ catalyst examined by Kubiak et al. under the same conditions, $E_{cat/2}$ is 100 mV less negative, while the current density is in a comparable range (see Table 4).[29] Since no significant Faradaic current was observed under the same conditions in the absence of **1** (black dotted line), the high cathodic current density can only originate from rapid catalytic

DOI: 10.1021/acscatal.8b03548
ACS Catal. 2019, 9, 2091−2100

reduction of CO_2 by the Mn complex. While the initial reduction $j_{1,red}$ remains as a (slightly enhanced) prepeak of the catalytic wave, the corresponding reoxidation peak $j_{1,ox}$ disappears. This behavior suggests that in the presence of CO_2, the cathodically generated doubly reduced species **6** is reoxidized in the reverse scan by the chemical reaction rather than by the electrode and thus must represent the active species in the catalytic process. The use of H_2O or MeOH instead of TFE had a similar impact on the voltammetry, whereby the catalytic wave was much less pronounced at the same proton donor concentrations and the maximum achievable currents were lower (see Figures S27–S31).[30,31]

The peaked shape of the catalytic wave indicates a limitation of j by either diffusion of CO_2 to the electrode and/or other side-effects such as product inhibition at potentials more negative than the peak potential of the catalytic wave.[32] In order to suppress such side effects, the scan rate and the substrate concentrations are often increased, allowing for the extraction of the pseudo-first-order rate constant TOF_{max}. In the ideal case, the formation of a current plateau indicates that no substrate is consumed and that the catalytic current is kinetically controlled. Since in our case this treatment leads to complications (for details see Supporting Information), we decided to analyze the onset of the catalytic wave where substrate diffusion, product inhibition, and other side effects do not play a role.[32] In order to extract the pseudo-first-order rate constant TOF_{max}, we used eq 1 reported in the literature ("foot-of-the-wave-analysis"),[33]

$$\frac{j}{j_p} = \frac{2.24\cdot\sqrt{\frac{RT}{Fv}}\cdot\sqrt{TOF_{max}}}{1+\exp\left(\frac{F}{RT}(E-E_{cat/2})\right)}\cdot\frac{n}{z^{3/2}} \quad (1)$$

which describes the catalytic current density j as a function of the applied electrode potential E (with j_p as the peak current density at $E = -1.02$ V under Ar, z the number of electrons transferred per catalyst unit under noncatalytic conditions ($z = 2$), and n the number of electrons required per turnover of one CO_2 molecule ($n = 2$). In order to improve the accuracy of the estimation, we applied the treatment to CVs recorded at various scan rates (see Figure 6, left). The slopes of the linearized j/j_p curves (top right) were extracted from the colored segments and plotted vs $v^{-1/2}$ in order to obtain TOF_{max} (bottom right), whereby for the latter a value of 40 s^{-1} was obtained. It is important to note that TOF_{max} refers only to the catalyst units which are present in the reaction-diffusion layer in the vicinity to the electrode and cannot be compared to macroscopic rate constants. A comparison to other Mn catalysts including a catalytic Tafel plot is provided in the SI.

In order to analyze the products of the electrocatalytic reduction, we carried out controlled potential electrolysis (CPE). Gas chromatography indicates that no hydrogen is formed during electrolysis and that CO is produced with almost quantitative selectivity (*vide infra*). The formation of water as byproduct was confirmed by Karl Fischer titration. Having the reaction products established, the overpotential η_{cat} required for catalysis with respect to the equilibrium potential E^0 for the CO_2/CO couple can be calculated according to eq 2.[34] Using the previously reported $E_0(CO_2/CO)$ value of −0.65 V vs NHE,[35] η_{cat} amounts to 0.64 V for our Mn catalyst, which is 100 mV less negative compared to [Mn(Mes-bpy)$(CO)_3(CH_3CN)$](OTf) and 140 mV less negative compared to [Mn(*t*Bu-bpy)$(CO)_3$Br].[23b,30a]

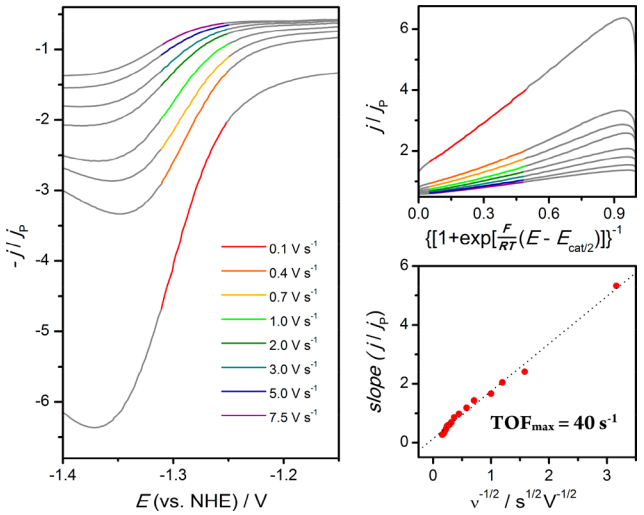

Figure 6. Foot-of-the-wave-analysis of the catalytic response at various v (same conditions as shown in Figure 5). The catalytic waves with v between 10 and 40 V s^{-1} were omitted for clarity (all scans are shown in the SI).

$$\eta_{cat} = |E^0(CO_2/CO) - E_{cat/2}| \quad (2)$$

Carrying out CPE experiments at $E = -1.2$ V (the potential of the onset of the catalytic wave) in a divided cell using a glassy carbon working electrode, CO was generated in >99% Faradaic efficiency (*FE*) (see Figure 7) with turnover numbers

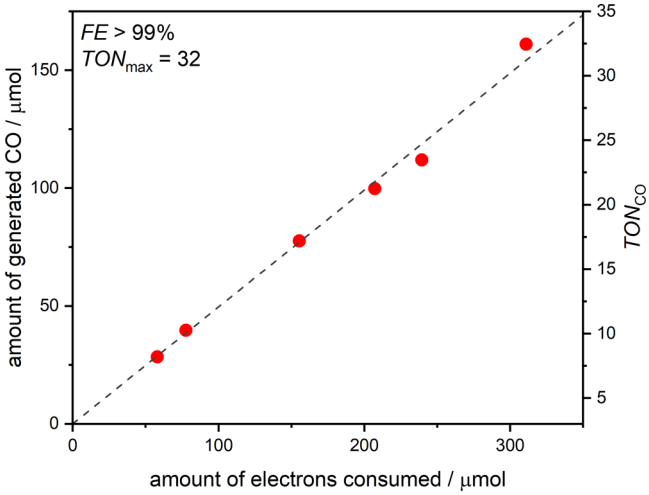

Figure 7. Electrocatalytic reduction of CO_2 using 1 mM **1** in the presence of 1 M TFE in controlled potential electrolysis ($E = -1.2$ V, electrolyte: 0.1 M NBu_4BF_4/CH_3CN): Plot of the amount of generated CO and the TON, respectively, vs the amount of passed charge (in μmol electrons).

(TON) up to 32 (for more details see SI). With initial current densities in the range between 3 and 4 mA cm^{-2}, the catalytic system displays activity for up to 8 h (Figure S37),[36] whereby an eventual decrease of j to a baseline (approximately 0.2 mA cm^{-2}) indicated complete catalyst deactivation. Further electrolyses were performed at −1.13 V and −1.35 V which both yielded CO in significantly lower FE and TON (for more details see Supporting Information).

It is important to note that the current density can be improved by increasing the catalyst loading, since j is directly

DOI: 10.1021/acscatal.8b03548
ACS Catal. 2019, 9, 2091−2100

proportional to the catalyst concentration (see Figure S32). For instance, an initial j of 18 mA cm^{-2} was obtained when the catalyst concentration was increased to 5 mM.

2.7. IR Spectroelectrochemical Investigations. To gain deeper knowledge about the mechanistic nature of the electrochemical CO_2-to-CO conversion, we carried out IR spectroelectrochemistry (SEC) at constant potential using a thin layer cell in the external reflection mode (for details see SI). The experiments were conducted in the presence of 1 mM **1** using a 0.1 M NBu_4PF_6/CH_3CN electrolyte and a glassy carbon working electrode under Ar (Figure 8) as well as under

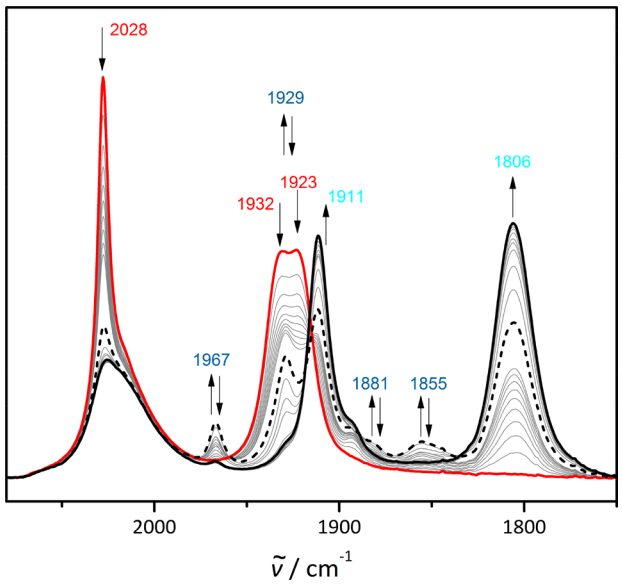

Figure 8. IR SEC of 1 mM **1** in CH_3CN at −1.45 V vs Ag wire under Ar: Progression of the absorption spectra over time. Red line: Initial spectrum of **1**. Black line: Final spectrum after completed reduction of **1**. The color coding of the absorption frequencies indicates their assignment to the species shown in Tables 3 and 5 (Red: species **1**, blue: species **4**, cyan: species **6**).

CO_2 (Figure 9). An Ag wire quasi reference electrode was used, and the potential adjusted to −1.45 V vs Ag wire in each experiment (recording a CV prior to the SEC experiment confirmed that this potential corresponds to a value slightly negative of the two-electron reduction wave of **1**).

Under argon atmosphere (Figure 8), holding the potential at −1.45 V leads to a diminution of the IR bands of **1** at 2028, 1932, and 1923 cm^{-1}, while six new bands are evolving. The signals at 1967, 1929, 1881, and 1855 cm^{-1} have already been observed in the photocatalytic *in situ* IR spectroscopy experiment (see Figure 4) and can be assigned to the Mn−Mn dimer **4**.[22,23] We assign the remaining two bands at 1911 and 1806 cm^{-1} to the doubly reduced Mn species **6** in good agreement with the IR spectrum of $[Mn(t\text{Bu-bpy})(CO)_3]^-$ reported in the literature (see Table 5).[23b]

The SEC results for the experiment conducted at −1.45 V vs Ag wire under CO_2 are shown in Figure 9. Again, a decrease of the bands of **1** concomitant with an increase of the bands corresponding to **4** and **6** was observed. Furthermore, a set of bands at 2037, 1940, 1914, and 1689 cm^{-1} appeared. These bands match the bicarbonate complex $[Mn(IMP)(CO)_3(HCO_3)]$ (IMP = 2-[(phenylimino)methyl]pyridine) reported in the literature,[22] and therefore we assign these bands to the bicarbonate complex **7** (see Table 5). The

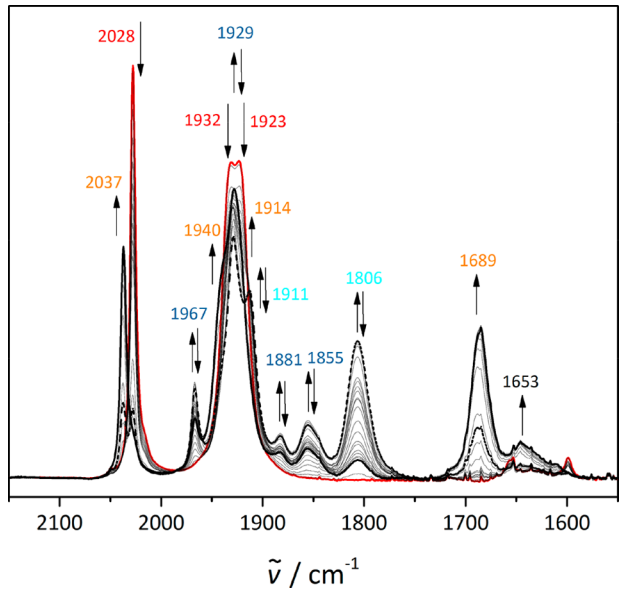

Figure 9. IR SEC of 1 mM **1** in CH_3CN at −1.45 V vs Ag wire under CO_2: Progression of the absorption spectra over time. Red line: Initial spectrum of **1b**. Black line: Final spectrum after reaching a steady state. The color coding of the absorption frequencies indicates their assignment to the species shown in Tables 3 and 5 (Red: species **1**, blue: species **4**, cyan: species **6**, orange: species **7**).

Table 5. Assignment of the IR Absorption Bands from Figures 8 and 9 to Electrocatalytic Intermediates Using Reference Spectra from the Literature

Species	$\tilde{\nu}$/cm^{-1}			
6				
$[Mn(pyrox)(CO)_3]^-$	1911	1806		
$[Mn(t\text{Bu-bpy})(CO)_3]^-$[23b]	1907	1807		
7				
$[Mn(pyrox)(CO)_3(HCO_3)]$	2037	1940	1914	1689
$[Mn(IMP)(CO)_3(HCO_3)]$[22]	2036	1940	1924	1671

assignment was also confirmed by a test reaction, where $NaHCO_3$ was added to a solution of the cationic species **5** in ethanol/water (2:1) (reaction monitoring via IR spectroscopy showed the corresponding shift of the $\tilde{\nu}_{CO}$ stretches). In addition, a band at 1653 cm^{-1} appeared, which can be attributed to uncoordinated bicarbonate resulting from the reaction between water formed in the catalytic process and CO_2. As in the photocatalytic experiments, uncoordinated CO was not detected due to the poor solubility of carbon monoxide in acetonitrile, which was used as solvent.[25]

3. MECHANISTIC PROPOSAL

On the basis of IR spectroscopic and spectroelectrochemical studies as well as the CV and quenching experiments, we propose a mechanism for the photo- and the electrochemical process (see Scheme 1). In each case, the sequence is initiated by reductive dehalogenation of catalyst precursor **1** leading to the radical species **4′**, which exists in equilibrium with the Mn−Mn dimer species **4** (notably, the dehalogenation may in parallel occur via solvolysis in the photochemical case). The reductive dehalogenation is followed by a second electron transfer to yield anionic intermediate **6**. Although the CV data shows that the radical intermediate **4′** is more easily reduced than dimer **4**, both species can in principle be reduced by the

DOI: 10.1021/acscatal.8b03548
ACS Catal. 2019, 9, 2091−2100

Scheme 1. Proposed Catalytic Cycles for the Photochemical and Electrochemical CO_2 Reduction Catalyzed by 1[a]

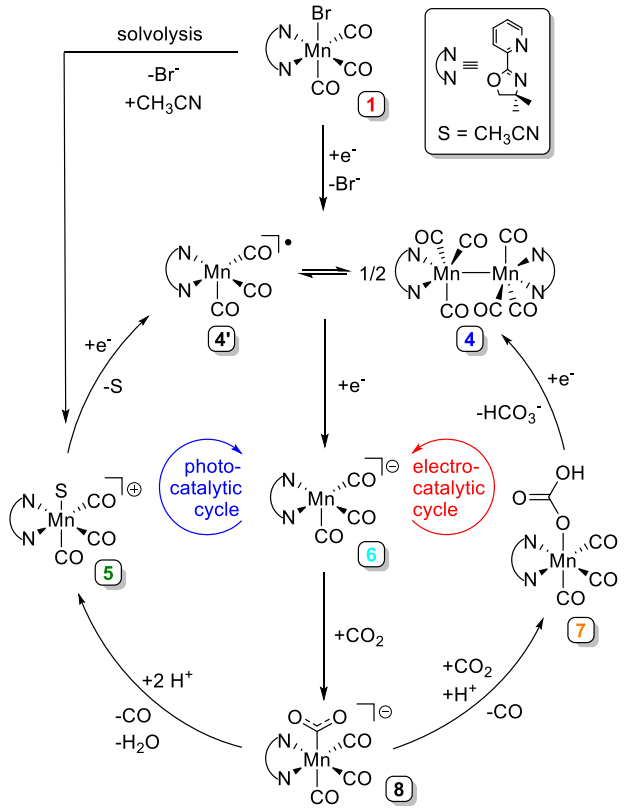

[a]The highlighted species were observed spectroscopically.

photosensitizer (E = −1.40 vs NHE)[37] and the applied electrolysis potential (E = −1.20 vs NHE), respectively. It is worth highlighting that in contrast to the SEC experiments, species **6** was not observed in the *in situ* IR photocatalytic study. We assume that differences in the experimental setup are responsible for the absence of the IR bands associated with **6**. In particular, the spatial separation between the photoreactor and the measuring cell, both connected to each other within a pump cycle, provides additional time for the quenching of **6** by CO_2.

The anionic intermediate **6** generated in the reduction step represents the active nucleophilic species which coordinates CO_2 to form metallacarboxylate species **8**. According to the IR spectroscopic results, intermediate **8** appears to be the point where the electrocatalytic and the photocatalytic pathways part: Under electrochemical conditions, a sequence involving reaction with a second CO_2 molecule, protonation, dehydration, and decarbonylation ultimately leads to the formation of the bicarbonate complex **7**, which is more difficult to reduce than catalyst precursor **1** and therefore responsible for the negative shift of the catalytic wave in the CV experiments. A similar negative shift of the catalytic wave for CO_2 reduction was recently reported by Hartl et al. employing Mn diimine complexes.[22] Under photochemical conditions, however, the solvent complex **5** was detected instead of **7**. A plausible explanation for this observation would be a protonation−dehydration−decarbonylation sequence, which ultimately leads to **5**. Since the reaction from **7** to **5** does not occur under electrochemical conditions (in the dark), we can conclude that the sequence must be light-induced. Reduction of **5** by the PS and of **7** by cathodic reduction, respectively, closes the catalytic cycle. In both the photo- and the electrocatalytic processes, IR spectroscopy in the presence of $^{13}CO_2$ confirmed that the CO ligands of the initial complex remain unaffected (for details see the Supporting Information). This observation also rules out the formation of a $[Mn(pyrox)(CO)_4]^+$ intermediate.[38] Consequently, the dehydration and the decarbonylation of protonated **8** must proceed in a concerted fashion. We note that in contrast to intermediates **4** − **7**, species **4′** and **8** were not detected presumably due to their transient nature.

4. CONCLUSIONS

In summary, we present a combined photo- and electrochemical study of the CO_2-to-CO conversion using a fully earth-abundant catalytic system. With our photochemical experiments we have shown that the use of $[Mn(pyrox)(CO)_3Br]$ under irradiation in combination with an *in situ* generated heteroleptic CuPS (Chart 1, bottom right) and BIH/TEOA as sacrificial reagents renders TONs up to 1058. Notably, this TON is among the highest values reported thus far within the group of fully earth abundant photocatalytic systems.

With respect to the economic and ecologic limitations associated with the use of stoichiometric amounts of SD, we have explored the possibility to transfer the same photocatalyst to an electrochemical process. We have shown that the PS, light source, and SD can indeed be replaced by a cathode and a weak Brønsted acid. In terms of chemoselectivity, both systems achieve values >99% with respect to CO formation. Regarding the achievable TONs, the outcome is clearly in favor of the photocatalytic method (1058 vs 32).

Mechanistically, the combined photo- and electrochemical approach proved to be beneficial for the understanding of both processes. Using a combination of different analytical methods, we identified the two-electron reduction of **1** to **6** (with a dimerization of intermediate **4′** to **4** as competing pathway) and subsequent formation of CO_2 adduct **8** as common steps. At this point, the catalytic cycles part, whereby the photochemical pathway proceeds via cationic intermediate **5** and the electrocatalytic one via the bicarbonate adduct **7**. The comparison between the two processes allows for the conclusion that in the dark, the metallacarboxylate **8** is rather activated by another CO_2 molecule, whereas in the photoreactor, a concerted light-induced dehydration-decarbonylation step changes the course of the reaction. Furthermore, the detection of the active species **6** in the SEC experiments allowed for the complementation of the mechanistic picture of the photochemical process, where **6** could not be observed due to the experimental restrictions of the standard *in situ* spectroscopic setup.

We believe that the present study contributes to the general understanding of the similarities and differences of photo- and electrocatalytical processes. An important goal for future research will be the development of more unifying concepts toward practically relevant applications.

■ ASSOCIATED CONTENT

Supporting Information

The Supporting Information is available free of charge on the ACS Publications website at DOI: 10.1021/acscatal.8b03548.

X-ray crystallographic data for compound **1** (CIF)

X-ray crystallographic data for compound **3** (CIF)

DOI: 10.1021/acscatal.8b03548
ACS Catal. 2019, 9, 2091−2100

Experimental procedures and spectra data for all new compounds, electro- and photocatalytic experiments. (PDF)

AUTHOR INFORMATION

Corresponding Authors

*E-mail: matthias.beller@catalysis.de.

*E-mail: robert.francke@uni-rostock.de.

ORCID

Robert Francke: 0000-0002-4998-1829

Matthias Beller: 0000-0001-5709-0965

Notes

The authors declare no competing financial interest.

ACKNOWLEDGMENTS

CS acknowledges financial support from EU fund H2020-MSCA-ITN-2015 in Horizon 2020 as part of the NoNoMeCat (Grant Agreement Number: 675020). RF is grateful for a Liebig Fellowship (Fonds der Chemischen Industrie). Additional financial support by the German Research Foundation (DFG, Grant No. FR 3848/1-1) is appreciated. We are also grateful to BMBF and to Mecklenburg - Vorpommern. We thank Peter Kumm for machining the spectroelectrochemical cell as well as Elisabetta Alberico and Alonso Rosas-Hernández for fruitful discussions and collaboration.

REFERENCES

(1) Yamazaki, Y.; Takeda, H.; Ishitani, O. Photocatalytic reduction of CO_2 using metal complexes. *J. Photochem. Photobiol., C* **2015**, *25*, 106−137.

(2) (2) Leitner, W. Carbon Dioxide as a Raw Material: The Synthesis of Formic Acid and its Derivatives from CO_2. *Angew. Chem., Int. Ed. Engl.* **1995**, *34*, 2207−2221. Artz, J.; Müller, T. E.; Thenert, K.; Kleinekorte, J.; Meys, R.; Sternberg, A.; Bardow, A.; Leitner, W. Sustainable Conversion of Carbon Dioxide: An Integrated Review of Catalysis and Life Cycle Assessment. *Chem. Rev.* **2018**, *118*, 434−504.

(3) (a) Hawecker, J.; Lehn, J.-M.; Ziessel, R. Photochemical and Electrochemical Reduction of Carbon Dioxide to Carbon Monoxide Mediated by (2,2′-Bipyridine)tricarbonylchlororhenium(I) and Related Complexes as Homogeneous Catalysts. *Helv. Chim. Acta* **1986**, *69*, 1990−2012. (b) Francke, R.; Roemelt, M.; Schille, B. Homogeneously Catalyzed Electroreduction of Carbon Dioxide-Methods, Mechanisms, and Catalysts. *Chem. Rev.* **2018**, *118*, 4631−4701. (c) Qiao, J.; Liu, Y.; Hong, F.; Zhang, J. A review of catalysts for the electroreduction of carbon dioxide to produce low-carbon fuels. *Chem. Soc. Rev.* **2014**, *43*, 631−675. (d) Benson, E. E.; Kubiak, C. P.; Sathrum, A. J.; Smieja, J. M. Electrocatalytic and homogeneous approaches to conversion of CO_2 to liquid fuels. *Chem. Soc. Rev.* **2009**, *38*, 89−99. (e) Costentin, C.; Robert, M.; Savéant, J.-M. Catalysis of the electrochemical reduction of carbon dioxide. *Chem. Soc. Rev.* **2013**, *42*, 2423−2436.

(4) Takeda, H.; Cometto, C.; Ishitani, O.; Robert, M. Electrons, Photons, Protons and Earth-Abundant Metal Complexes for Molecular Catalysis of CO2 Reduction. *ACS Catal.* **2017**, *7*, 70−88.

(5) (a) Valeur, B. *Molecular Fluorescence − Principles and Applications* Wiley-VCH: Weinheim, 2002; p 56. (b) Koike, T.; Akita, M. Visible-light radical reaction designed by Ru- and Ir-based photoredox catalysis. *Inorg. Chem. Front.* **2014**, *1*, 562−576.

(6) (a) Hawecker, J.; Lehn, J.-M.; Ziessel, R. Electrocatalytic reduction of carbon dioxide mediated by $Re(bipy)(CO)_3Cl$ (bipy = 2,2′-bipyridine). *J. Chem. Soc., Chem. Commun.* **1984**, 328−330. (b) Sullivan, B. P.; Bolinger, C. M.; Conrad, D.; Vining, W. J.; Meyer, T. J. One- and two-electron pathways in the electrocatalytic reduction of CO2 by fac-Re(bpy)(CO)3Cl (bpy = 2,2′-bipyridine). *J. Chem. Soc., Chem. Commun.* **1985**, 1414−1416.

(7) Ishida, H.; Tanaka, K.; Tanaka, T. Electrochemical CO_2 reduction catalyzed by ruthenium complexes $[Ru(bpy)_2(CO)_2]^{2+}$ and $[Ru(bpy)_2(CO)Cl]^+$. Effect of pH on the formation of CO and HCOO-. *Organometallics* **1987**, *6*, 181−186.

(8) Rakowski Dubois, M.; Dubois, D. L. Development of Molecular Electrocatalysts for CO_2 Reduction and H_2 Production/Oxidation. *Acc. Chem. Res.* **2009**, *42*, 1974−1982.

(9) (a) Rosas-Hernández, A.; Junge, H.; Beller, M.; Roemelt, M.; Francke, R. Cyclopentadienone iron complexes as efficient and selective catalysts for the electroreduction of CO_2 to CO. *Catal. Sci. Technol.* **2017**, *7*, 459−465. (b) Oberem, E.; Roesel, A. F.; Rosas-Hérnandez, A.; Kull, T.; Fischer, S.; Spannenberg, A.; Junge, H.; Beller, M.; Ludwig, R.; Roemelt, M.; Francke, R. Mechanistic Insights into the Electrochemical Reduction of Carbon Dioxide Catalyzed by Cyclopentadienone Iron Complexes. *Organometallics* **2018**, DOI: 10.1021/acs.organomet.8b00517. (c) Azcarate, I.; Costentin, C.; Robert, M.; Savéant, J.-M. Through-Space Charge Interaction Substituent Effects in Molecular Catalysis Leading to the Design of the Most Efficient Catalyst of CO_2-to-CO Electrochemical Conversion. *J. Am. Chem. Soc.* **2016**, *138*, 16639−16644. (d) Loewen, N. D.; Neelakantan, T. V.; Berben, L. A. Renewable Formate from C-H Bond Formation with CO_2: Using Iron Carbonyl Clusters as Electrocatalysts. *Acc. Chem. Res.* **2017**, *50*, 2362−2370.

(10) (a) Schneider, J.; Jia, H.; Kobiro, K.; Cabelli, D. E.; Muckerman, J. T.; Fujita, E. Nickel(II) macrocycles: highly efficient electrocatalysts for the selective reduction of CO_2 to CO. *Energy Environ. Sci.* **2012**, *5*, 9502−9510. (b) Froehlich, J. D.; Kubiak, C. P. The Homogeneous Reduction of CO_2 by $[Ni(cyclam)]^+$: Increased Catalytic Rates with the Addition of a CO Scavenger. *J. Am. Chem. Soc.* **2015**, *137*, 3565−3573.

(11) (a) Elgrishi, N.; Chambers, M. B.; Artero, V.; Fontecave, M. Terpyridine complexes of first row transition metals and electrochemical reduction of CO_2 to CO. *Phys. Chem. Chem. Phys.* **2014**, *16*, 13635−13644. (b) Roy, S.; Sharma, B.; Pecaut, J.; Simon, P.; Fontecave, M.; Tran, P. D.; Derat, E.; Artero, V. Molecular Cobalt Complexes with Pendant Amines for Selective Electrocatalytic Reduction of Carbon Dioxide to Formic Acid. *J. Am. Chem. Soc.* **2017**, *139*, 3685−3696.

(12) Bourrez, M.; Molton, F.; Chardon-Noblat, S.; Deronzier, A. $[Mn(bipyridyl)(CO)_3Br]$: an abundant metal carbonyl complex as efficient electrocatalyst for CO_2 reduction. *Angew. Chem., Int. Ed.* **2011**, *50*, 9903−9906.

(13) Takeda, H.; Koizumi, H.; Okamoto, K.; Ishitani, O. Photocatalytic CO_2 reduction using a Mn complex as a catalyst. *Chem. Commun.* **2014**, *50*, 1491−1493.

(14) Zhang, J.-X.; Hu, C.-Y.; Wang, W.; Wang, H.; Bian, Z.-Y. Visible light driven reduction of CO_2 catalyzed by an abundant manganese catalyst with zinc porphyrin photosensitizer. *Appl. Catal., A* **2016**, *522*, 145−151.

(15) Takeda, H.; Ohashi, K.; Sekine, A.; Ishitani, O. Photocatalytic CO_2 Reduction Using Cu(I) Photosensitizers with a Fe(II) Catalyst. *J. Am. Chem. Soc.* **2016**, *138*, 4354−4357.

(16) Rosas-Hernández, A.; Steinlechner, C.; Junge, H.; Beller, M. Earth-abundant photocatalytic systems for the visible-light-driven reduction of CO_2 to CO. *Green Chem.* **2017**, *19*, 2356−2360.

(17) Takeda, H.; Cometto, C.; Ishitani, O.; Robert, M. Electrons, Photons, Protons and Earth Abundant Metal Complexes for Molecular Catalysis of CO_2 Reduction. *ACS Catal.* **2017**, *7*, 70−88.

(18) Guo, Z.; Cheng, S.; Cometto, C.; Anxolabéhère-Mallart, E.; Ng, S.-M.; Ko, C.-C.; Liu, G.; Chen, L.; Robert, M.; Lau, T.-C. Highly Efficient and Selective Photocatalytic CO_2 Reduction by Iron and Cobalt Quaterpyridine Complexes. *J. Am. Chem. Soc.* **2016**, *138*, 9413−9416.

(19) (a) We note that BIH provides only one of the two required protons for the CO_2-to-CO conversion. This behavior was first reported by Ishitani et al., who also found that BIH is much more effective in the presence of TEOA due to the reaction $BIH^{\bullet+}$ + TEAO → $BI^{\bullet}$ + $TEOAH^+$ (see refs 19b and 19c). We observed the same behavior in the control experiment shown in Table 2, entry 8.

DOI: 10.1021/acscatal.8b03548
ACS Catal. 2019, 9, 2091−2100

(b) Sahara, G.; Ishitani, O. Efficient Photocatalysts for CO_2 Reduction. *Inorg. Chem.* **2015**, *54*, 5096−5104. (c) Tamaki, Y.; Koike, K.; Morimoto, T.; Ishitani, O. Substantial improvement in the efficiency and durability of a photocatalyst for carbon dioxide reduction using a benzoimidazole derivative as an electron donor. *J. Catal.* **2013**, *304*, 22−28.

(20) (a) Fischer, S.; Hollmann, D.; Tschierlei, S.; Karnahl, M.; Rockstroh, N.; Barsch, E.; Schwarzbach, P.; Luo, S.-P.; Junge, H.; Beller, M.; Lochbrunner, S.; Ludwig, R.; Brückner, A. Death and Rebirth: Photocatalytic Hydrogen Production by a Self-Organizing Copper−Iron System. *ACS Catal.* **2014**, *4*, 1845−1849. (b) Armaroli, N.; Accorsi, G.; Cardinali, F.; Listorti, A. Photochemistry and Photophysics of Coordination Compounds. *Top.Curr. Chem.* **2007**, *280*, 69−115.

(21) (a) Niaura, G. Surface-enhanced Raman spectroscopic observation of two kinds of adsorbed OH^- ions at copper electrode. *Electrochim. Acta* **2000**, *45*, 3507−3519. (b) Deng, Y.; Handoko, A. D.; Du, Y.; Xi, S.; Yeo, B. S. *In Situ* Raman Spectroscopy of Copper and Copper Oxide Surfaces during Electrochemical Oxygen Evolution Reaction: Identification of CuIII Oxides as Catalytically Active Species. *ACS Catal.* **2016**, *6*, 2473−2481.

(22) Spall, S. J. P.; Keane, T.; Tory, J.; Cocker, D. C.; Adams, H.; Fowler, H.; Meijer, A. J. H. M.; Hartl, F.; Weinstein, J. A. Manganese Tricarbonyl Complexes with Asymmetric 2-Iminopyridine Ligands: Toward Decoupling Steric and Electronic Factors in Electrocatalytic CO_2 Reduction. *Inorg. Chem.* **2016**, *55*, 12568−12582.

(23) (a) Franco, F.; Cometto, C.; Nencini, L.; Barolo, C.; Sordello, F.; Minero, C.; Fiedler, J.; Robert, M.; Gobetto, R.; Nervi, C. Local Proton Source in Electrocatalytic CO_2 Reduction with $[Mn(bpy-R)(CO)_3Br]$ Complexes. *Chem. - Eur. J.* **2017**, *23*, 4782−4793. (b) Smieja, J. M.; Sampson, M. D.; Grice, K. A.; Benson, E. E.; Froehlich, J. D.; Kubiak, C. P. Manganese as a Substitute for Rhenium in CO_2 Reduction Catalysts: The Importance of Acids. *Inorg. Chem.* **2013**, *52*, 2484−2491.

(24) (a) Cheng, S. C.; Blaine, C. A.; Hill, M. G.; Mann, K. R. Electrochemical and IR Spectroelectrochemical Studies of the Electrocatalytic Reduction of Carbon Dioxide by $[Ir_2(dimen)_4]^{2+}$ (dimen = 1,8-Diisocyanomenthane). *Inorg. Chem.* **1996**, *35*, 7704−7708. (b) Garand, E.; Wende, T.; Goebbert, D. J.; Bergmann, R.; Meijer, G.; Neumark, D. M.; Asmis, K. R. Infrared Spectroscopy of Hydrated Bicarbonate Anion Clusters: $HCO_3^-(H_2O)_{1-10}$. *J. Am. Chem. Soc.* **2010**, *132*, 849−856. (c) Johnson, B. A.; Maji, S.; Agarwala, H.; White, T. A.; Mijangos, E.; Ott, S. Activating a Low Overpotential CO_2 Reduction Mechanism by a Strategic Ligand Modification on a Ruthenium Polypyridyl Catalyst. *Angew. Chem.* **2016**, *128*, 1857−1861.

(25) Lopez-Castillo, Z. K.; Aki, S. N. V. K.; Stadtherr, M. A.; Brennecke, J. F. Enhanced Solubility of Oxygen and Carbon Monoxide in CO_2-Expanded Liquids. *Ind. Eng. Chem. Res.* **2006**, *45*, 5351−5360.

(26) Berardi, S.; Drouet, S.; Francás, L.; Gimbert-Surinach, C.; Guttentag, M.; Richmond, C.; Stoll, T.; Llobet, A. Molecular artificial photosynthesis. *Chem. Soc. Rev.* **2014**, *43*, 7501−7519.

(27) Li, T.; Cao, Y.; He, J.; Berlinguette, C. P. Electrolytic CO_2 Reduction in Tandem with Oxidative Organic Chemistry. *ACS Cent. Sci.* **2017**, *3*, 778−783.

(28) Llorente, M. J.; Nguyen, B. H.; Kubiak, C. P.; Moeller, K. D. Paired Electrolysis in the Simultaneous Production of Synthetic Intermediates and Substrates. *J. Am. Chem. Soc.* **2016**, *138*, 15110−15113.

(29) Chen, Z.; Concepcion, J. J.; Brennaman, M. K.; Kang, P.; Norris, M. R.; Hoertz, P. G.; Meyer, T. J. Splitting CO_2 into CO and O_2 by a single catalyst. *Proc. Natl. Acad. Sci. U. S. A.* **2012**, *109*, 15606−15611.

(30) (a) Sampson, M. D.; Nguyen, A. D.; Grice, K. A.; Moore, C. E.; Rheingold, A. L.; Kubiak, C. P. Manganese Catalysts with Bulky Bipyridine Ligands for the Electrocatalytic Reduction of Carbon Dioxide: Eliminating Dimerization and Altering Catalysis. *J. Am. Chem. Soc.* **2014**, *136*, 5460−5471. (b) Ngo, K. T.; McKinnon, M.; Mahanti, B.; Narayanan, R.; Grills, D. C.; Ertem, M. Z.; Rochford, J. Turning on the Protonation-First Pathway for Electrocatalytic CO_2 Reduction by Manganese Bipyridyl Tricarbonyl Complexes. *J. Am. Chem. Soc.* **2017**, *139*, 2604−2618.

(31) It is worth mentioning that the use of phenol as proton source led to catalytic currents which are comparable to the ones obtained using TFE (see SI). Since the Faradaic yields in controlled potential electrolyses were lower when phenol was used, we decided to focus on TFE as proton donor throughout this study.

(32) Costentin, C.; Drouet, S.; Robert, M.; Savéant, J.-M. Turnover Numbers, Turnover Frequencies, and Overpotential in Molecular Catalysis of Electrochemical Reactions. Cyclic Voltammetry and Preparative-Scale Electrolysis. *J. Am. Chem. Soc.* **2012**, *134*, 11235−11242.

(33) (a) Costentin, C.; Savéant, J.-M. Multielectron, Multistep Molecular Catalysis of Electrochemical Reactions: Benchmarking of Homogeneous Catalysts. *ChemElectroChem* **2014**, *1*, 1226−1236. (b) Rountree, E. S.; McCarthy, B. D.; Eisenhart, T. T.; Dempsey, J. L. Evaluation of Homogeneous Electrocatalysts by Cyclic Voltammetry. *Inorg. Chem.* **2014**, *53*, 9983−10002.

(34) Appel, A. M.; Helm, M. L. Determining the Overpotential for a Molecular Electrocatalyst. *ACS Catal.* **2014**, *4*, 630−633.

(35) Costentin, C.; Drouet, S.; Robert, M.; Savéant, J.-M. A local proton source enhances CO_2 electroreduction to CO by a molecular Fe catalyst. *Science* **2012**, *338*, 90−94.

(36) The TOF_{max} value calculated from the electrolysis current is in agreement with the value obtained using the foot-of-the-wave analysis (for details see Supporting Information).

(37) Mejía, E.; Luo, S.-P.; Karnahl, M.; Friedrich, A.; Tschierlei, S.; Surkus, A.-E.; Junge, H.; Gladiali, S.; Lochbrunner, S.; Beller, M. A Noble-Metal-Free System for Photocatalytic Hydrogen Production from Water. *Chem. - Eur. J.* **2013**, *19*, 15972−15978.

(38) Protonation and dehydration of **8** lead to $[Mn(pyrox)(CO)_4]^+$, wherein both axial CO ligands are weakly bound and prone to cleavage. Since in the labeling experiment a shift of the axial $\tilde{\nu}_{CO}$ stretch in intermediate **5** was not observed, the formation of a tetracarbonyl intermediate can be ruled out.

DOI: 10.1021/acscatal.8b03548
ACS Catal. 2019, 9, 2091−2100